processes

MDPI

Article

Simulation and Experimental Validation on the Effect of Twin-Screw Pulping Technology upon Straw Pulping Performance Based on Tavares Mathematical Model

Huiting Cheng, Yuanjuan Gong, Nan Zhao, Luji Zhang, Dongqing Lv and Dezhi Ren *

College of Engineering, Shenyang Agricultural University, Shenyang 110866, China
* Correspondence: rdz@syau.edu.cn; Tel.: +86-138-8921-5226

Abstract: Rice straw is waste material from agriculture as a renewable biomass resource, but the black liquor produced by straw pulping causes serious pollution problems. The twin-screw pulping machine was designed by Solidworks software and the straw breakage model was created by the Discrete Element Method (DEM). The model of straw particles breakage process in the Twin-screw pulping machine was built by the Tavares model. The simulation results showed that the highest number of broken straw particles was achieved when the twin-screw spiral casing combination was negative-positive-negative-positive and the tooth groove angle arrangement of the negative spiral casing was 45°−30°−15°. The multi-factor simulation showed that the order of influence of each factor on the pulp yield was screw speed > straw moisture content > tooth groove angle. The Box-Behnken experiment showed that when screw speed was 550 r/min, tooth groove angle was 30°, straw moisture content was 65% and pulping yield achieved up to 92.5%. Twin-screw pulping performance verification experiments were conducted, and the results from the experimental measurements and simulation data from the model showed good agreement.

Keywords: twin-screw pulping; semi-dry pulping; straw breakage; Discrete Element Method; Tavares model

check for updates

Citation: Cheng, H.; Gong, Y.; Zhao, N.; Zhang, L.; Lv, D.; Ren, D. Simulation and Experimental Validation on the Effect of Twin-Screw Pulping Technology upon Straw Pulping Performance Based on Tavares Mathematical Model. *Processes* **2022**, *10*, 2336. https://doi.org/10.3390/pr10112336

Academic Editors: Shicheng Zhang, Gang Luo, Abdul-Sattar Nizami, Andrzej Bialowiec and Yan Shi

Received: 16 October 2022
Accepted: 8 November 2022
Published: 9 November 2022

Publisher's Note: MDPI stays neutral with regard to jurisdictional claims in published maps and institutional affiliations.

Copyright: © 2022 by the authors. Licensee MDPI, Basel, Switzerland. This article is an open access article distributed under the terms and conditions of the Creative Commons Attribution (CC BY) license (https://creativecommons.org/licenses/by/4.0/).

1. Introduction

China's rice planted area and straw yield are large [1], and the utilization rate of straw fertilization, feederization and fuelization are relatively high, while the utilization rate of raw materialization is only 1.0% [2]. Traditional pulping methods have led to a wood shortage and environmental pollution, and straw as a wasted crop can become an alternative method of pulping [3]. Straw pulping has an important role in the Chinese pulping industry, but the complex structure of straw leads to black liquor produced in the pulping process and increases pollution emissions [4]. Therefore, the simulation and experimental study of pulping performance is important to improve the utilization rate of straw raw materialization and promote clean straw pulping.

The Discrete Element Method (DEM) can simulate the motion of individual particles in granular media, and the Tavares model is a practical model to describe the fragmentation of individual particles, which is applied in the fields of particle fragmentation and material wear [5]. The particles under loading assume the following states: unbroken, worn, broken, and separated. DEM solves the particle motion problem based on Newton's equations of motion and uses the contact law to analyze the contact forces between the particles. Tavares proposes a practical model to describe the breakage of a single particle that can be used to describe the breakage of polyhedral particles when exposed to different intensity stresses [6]. The Tavares model was based on the research of Professor L.M. Tavares at the University of Utah and was developed through further research by a research group at the Federal University of Rio de Janeiro [5]. The Tavares model determines whether a particle would crush by calculating the energy displaced in the contact of two elements, and could simulate

the breakage of a particle under insufficient stress, explaining the probability of particle breakage through the upper truncated log-normal distribution. The Tavares model extends the breakage distribution function based on simple crushing, enabling breakage prediction to reach a more realistic level, contributing to the description of particle degradation during treatment and particle size reduction under different conditions. It can predict fracture and broken particle percentages for repeated impacts, based on a weakened model of continuum damage mechanics. Considering the special case of materials exhibiting a non-normalized fracture response, it describes the size distribution of particle breakage generations in terms of an incomplete beta function, which predicts the size distribution of fragments produced by stress events by describing experiential expressions for stress energy and fragmentation strength [7]. Currently, the Tavares fracture model is embedded in commercial DEM software (RockyDEM and Altair EDEM) and employed to simulate many complex industrial processes and integrated into micro-scale population balance models describing mill types.

Further, Barrios [8] simulated the fragmentation of the ironstone particle layer shock and compression loading by a DEM-coupled particle replacement model, which was able to describe the force and deformation profile generated by the individual particle loading, deriving a function for calculating the particle size based on the median ratio fracture energy. Carvalho [9] proposed a mathematical model for material grinding, describing the phenomena of fragmentation, wear, and repeated shock caused by the grinding medium, and accurately calculated the wear rate of both materials during the grinding process. Oliveira and Rodriguez [10] simulated the process of material crushing in a vertical stirred mill with a mechanical wear model and predicted the mill power by the Discrete Element Method with an error of less than 3.5% between simulation and experiment, proving that DEM can be used as a tool to predict and analyze the crushing behavior of materials. Tavares and Rodriguez [11] verified the effects of particle fracture energy, particle size, and material properties on the variation in the impact surface by comparing model predictions with single-particle fragmentation, showing that the model could accurately predict the distribution of fragments. Zeng and Mao [12] proposed a numerical method combining the Discrete Element Method (DEM) and the Particle Replacement Model (PRM) to compare the particle crushing process of the simulated vertical mill with the actual grinding process, and concluded that the simulation results were in agreement with the experimental results. Xu [13] used the coupling method of DEM to analyze the contact action between seeds and soil from a microscopic perspective and analyzed the influence of seed displacement during soil cover and compaction processing to verify the feasibility and applicability of the coupling method.

However, the main problems in the straw pulping industry are that it is hard to degrade lignin, chemical pulping is environmentally unfriendly, twin-screw pulping consumes the least energy among mechanical pulping methods, and biological pulping technology is not yet well established [14]. Therefore, the combination of biological and mechanical methods to degrade lignin for pulping is an efficient and environmentally friendly method [15]. At present, the research on twin-screw pulping machines mainly focuses on the optimization of twin-screw structure parameters and process conditions, while there is little research on the simulation of the straw breakage process. Xiaoyang [16] studied the influences of screw speed, inverted thread lead number and groove width of negative spiral casing on specific energy and pulping quality, but failed to consider the influence of tooth groove angle of negative spiral casing on pulping performance. Pradhan [17] conducted material crushing experiments to show that the geometry of the screw element affects the material particle crushing process, modifying the geometry of the screw element to change the size of the largest particle. Shirazian [18] constructed a two-dimensional population balance model (PBM) to find out the twin-screw pelletizing mechanism and carried out experiments on a 12 mm twin-screw with microcrystalline cellulose as the model to predict the GSD values at different spatial locations. Bumm [19] researched the damage to glass fiber of different viscosity and screw speeds, and estab-

lished a composite modular dynamics model to describe glass fiber fragmentation and compared the simulation results with experimental data to show a consistent relationship. Fleur Rol [20] used a twin-screw extruder to produce CNFs and compared it to an ultrafine grinder (UFG) and found that cellulose pulping with four passes of TSE reduced energy consumption by 4–5 times compared to UFG on the same mass index. Dyna Thenga [21] compared the energy consumption, extrudate and pulping properties of two pretreatment technologies, twin-screw extrusion and steam digestion. It found that twin-screw pulping demanded lower water volume, lower temperature, and lower energy consumption. Thu Ho [22] studied the effect of the fibrillation process on fiber properties in a twin-screw machine, where cellulose fibers were found to exhibit not only fibrillation but also some degree of degradation after several successive passes through the TSE. The method of twin-screw pulping has the advantage of low cost and high fiber content compared to other pulping mechanical methods. Ke pa [23] conducted twin-screw extrusion (TSE), high-energy ball milling (HEBM) and high-pressure homogenization (HPH) of alkali-treated material to convert into cellulose microfiber (MFC) and nanofiber (CNF), and fiber analysis using confocal laser scanning microscopy resulted in the lowest TSE energy consumption. Eduardo Espinosa [24] compared the energy consumption of Twins Screw Extruder (TSE), High Pressure Homogenizer (HPH) and Ultrafine Grinder (UFG) to describe the morphology, crystallinity, thermal stability, chemical structure and mechanical properties of the obtained lignocellulose. Twin-screw pulping was found to consume five times less energy than HPH and UFG. Fangmin Liang [25] used a low-cost Twins Screw Extruder (TSE) for bamboo pulping instead of the high-cost common extrusion Model Screw Device (MSD). TSE extruded material had shorter fibers, higher fines content, lower kink and curl indices compared to MSD, and the absorbance of TSE extruded material (4.50 g/g) was 3 times higher than that of MSD extruded material.

Material characteristics and structural parameters of the twin-screw pulping machine have an important influence on the straw pulping performance. In this work, the Discrete Element Model of straw crushing is created for the pulping process of rice straw in a twin-screw pulping machine based on the Tavares mathematical model, and the number of straw particles broken was analyzed. Ternary quadratic orthogonal center-of-rotation combination tests were conducted with rice straw pretreated using white rot fungi liquid as the experimental object, the straw pulping yield as evaluation indexes, and tooth groove angle, screw speed and straw moisture content as influencing factors, to improve the twin-screw pulp yield and the quality of the pulp without producing black liquor, to ensure a clean and efficient straw process.

2. Materials and Methods

The designed geometric model of the twin-screw pulping machine was imported into Rocky, the particle model of rice straw was set, the Tavares model was selected as the breakage model, and the sum of all forces and moments acting on the particles was calculated. The straw particle was moved to the next position until the end of the simulation, the position, velocity, and time step of the particle were calculated by the Rocky programs, and the simulation results were derived and verified. Based on the results of the simulation analysis, the twin-screw pulping machine was continually optimized until an optimal design was obtained. Multi-factor test with tooth groove angle, screw speed and straw moisture content as influencing factors, to explore the effect of each parameter on the pulping performance of the twin-screw machine, as shown in Figure 1.

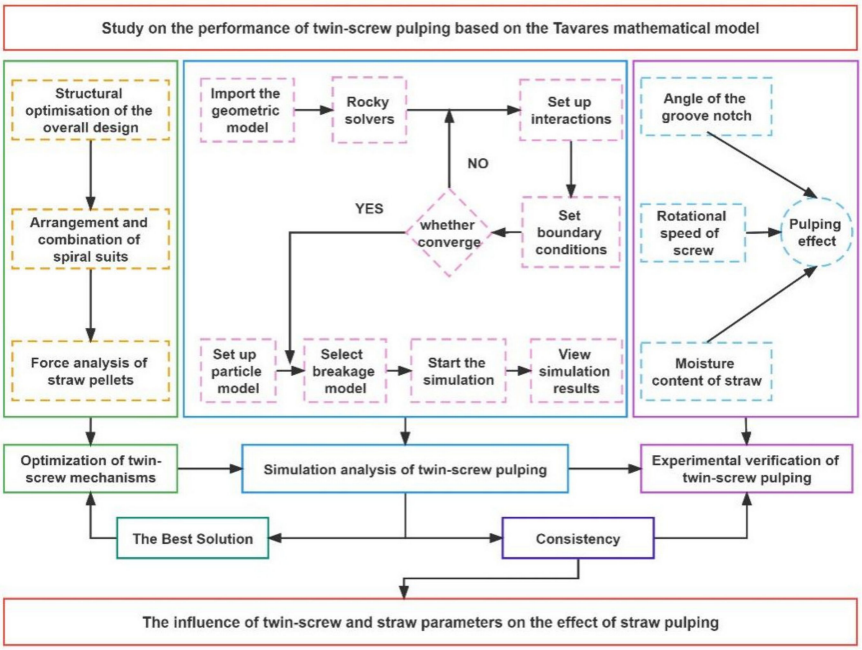


Figure 1. Process of twin-screw pulping simulation and experimental study.

2.1. Experimental Setup

2.1.1. Establishing a Mathematical Model of Twin-Screw Pulping Machine

The 3D model software named Solidworks was used to design and optimize the twin-screw pulping machine, which included screw discharge device, twin-screw device, screw feed device, rigid bearing chock, decelerator, coupling, drive motor, and body frame, as shown in Figure 2.

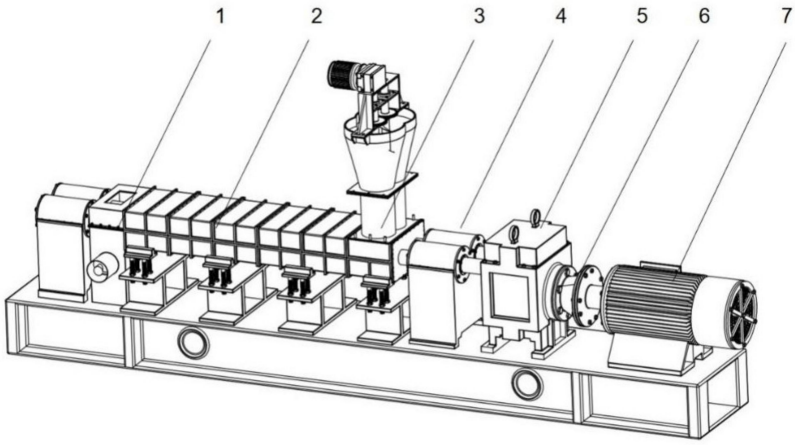


Figure 2. Structure of the twin-screw pulping machine. 1. screw discharge device; 2. twin-screw device; 3. screw feed device; 4. rigid bearing chock; 5. decelerator; 6. coupling; 7. drive motor.

The key component of pulping machinery, the twin-screw device, comprised of the positive spiral casing, negative spiral casing, conveying spiral casing and rotating shaft, as shown in Figure 3.

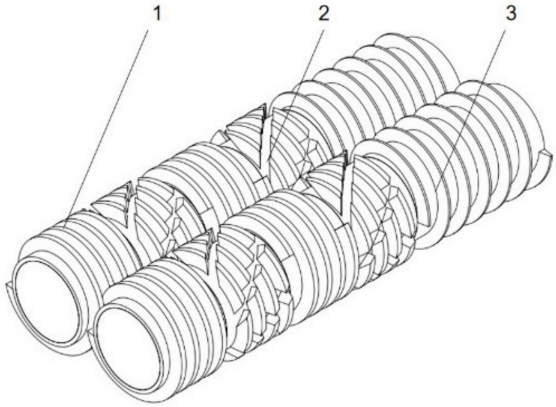


Figure 3. Twin-screw device. 1. positive spiral casing; 2. negative spiral casing; 3. conveying spiral casing.

The force on the straw through the positive spiral casing and the negative spiral casing formed a balanced force system to achieve the purpose of extrusion and shear [26]. The negative spiral casing was designed with the multi-headed reversal spiral groove, and the straw generated shear force and squeezing pressure when passing through the groove of the tooth. The equation of force on the tooth groove is:

$$\begin{cases} F_n = F_n \times \cos\alpha_n \times \sin_\gamma \\ F_{r1} = F_n \times \sin_n \\ F_{a1} = F_n \times \cos\alpha_n \times \cos_\gamma \end{cases} \quad (1)$$

2.1.2. Twin-Screw Structure Arrangement

In order to optimize the pulping performance of the twin-screw pulping device, the positive spiral casing and negative spiral casing were arranged in different combinations, which made the shearing rate, cumulative strain and specific mechanical energy of the straw material achieved the best value [27], as shown in Figure 4.

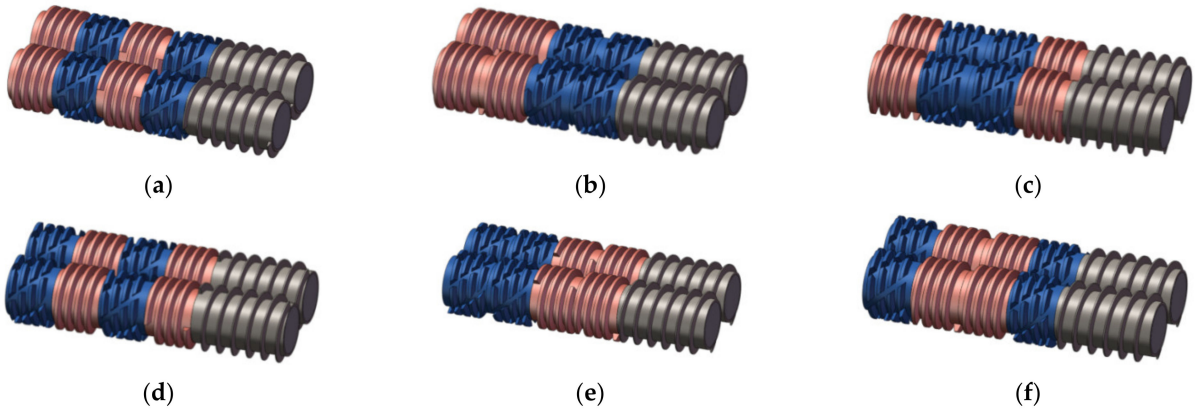


Figure 4. Combination of twin-screw mechanism spiral casing. (**a**) Positive-Negative-Positive-Negative (PNPN); (**b**) Positive-Positive-Negative-Negative (PPNN); (**c**) Positive-Negative-Negative-Positive (PNNP); (**d**) Negative-Positive-Negative-Positive (NPNP); (**e**) Negative-Negative-Positive-Positive (NNPP); (**f**) Negative-Positive-Positive-Negative (NPPN).

The specific mechanical energy (*SEM*) is calculated as follows:

$$SEM\left[\frac{KWh}{t}\right] = \frac{N * C * P_{\max}}{N_{\max} * C_{\max} * Q} \quad (2)$$

where N (r/min) and N_{max} (r/min) are the rotational speed of the screw and the maximum speed of the screw; P_{max} (7 kW) is the maximum power of the motor; C (N·m) and C_{max} (130 N·m) are torque and maximum torque; Q (t/h) is total flow.

2.1.3. Force Analysis of Straw Particles

1. Force analysis of twin-screw on straw particles;

Due to the complex force interaction of straw particles in the extrusion-shear section of the negative spiral casing [28], assuming a single screw as the object of study and straw particles as a whole, when the straw particles moved in the twin-screw pulping device, the force on each micro-element could be decomposed into 8 partial forces, as shown in Figure 5.

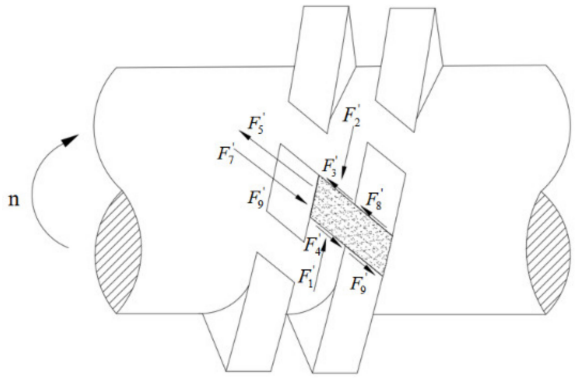


Figure 5. Force Analysis on the straw particles in the negative spiral casing. Where F_1', F_3', F_4', F_5' are friction forces; F_2', F_7' are extrusion forces; F_8', F_9' are shear forces.

A is the friction force of the screw surface on the straw particles, which is the driving force of the movement of the straw material flow in the screw teeth grooves, and is calculated as follows:

$$F_1' = f_b P S_b dL_b \tag{3}$$

where f_b is friction coefficient between screw surface and straw particles; P (Pa) is the pressure of straw particles on screw shaft; dL_b (mm) is the micro increments of the screw surface along the helix direction; S_b (mm^2) is the contact area between straw particles and screw.

2. Force analysis between straw particles;

The action model between the straw particles is the BPM bonding model, where the contact part between the particles of rice straw produces parallel bonding, which is equivalent to setting a set of springs on the circular section of the straw particles [29]. The force analysis between the particles is shown in Figure 6.

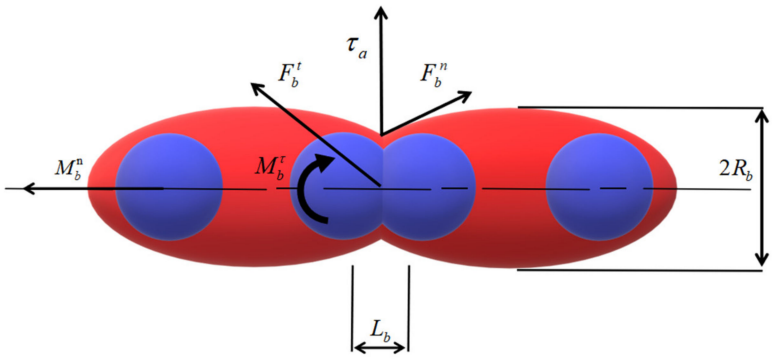


Figure 6. Force Analysis on the straw particles.

The torque of the rice straw particles is determined by Newton's second law, and the contact force between the particles due to relative motion is calculated by the force-displacement law [30]. The force equation of the straw particles is:

$$\begin{array}{l} \delta F_b^n = -\nu_n S_n A \delta t \\ \delta F_b^t = -\nu_t S_t A \delta t \\ \delta M_b^n = -\omega_n S_t J \delta t \\ \delta M_b^t = -\omega_n S_n \frac{J}{2} \delta t \end{array} \quad (4)$$

where δt (s) is time step; ν_n (m/s) and ν_t (m/s) are normal and tangential velocities of particles; ω_n (r/min) and ω_t (r/min) are normal and tangential angular velocities of particles; J (kg·m^2) is moment of inertia; A (mm^2) is contact area; S_n (N/m) and S_t (N/m) are normal stiffness and tangential stiffness per unit area.

2.2. Simulation Test

2.2.1. Simulation Model

In the Tavares breakage model, the fragmentation probability is based on the upper truncated log-normal distribution [31]. When a particle collision event occurs, the breakage ratio energy decreases owing to the accumulated damage to the particle during loading. When the particle is broken, the geometry of the fragments is generated by the Voronoi fracture equation and distributed according to the Gaudin-Schumann function.

The breakage probability expression is:

$$P_o(e) = \frac{1}{2}\left[1 + erf\left(\frac{\ln e^* - \ln e_{50}}{\sqrt{2\delta^2}}\right)\right] \quad (5)$$

where e^*(J) is relative breakage energy; e_{50} (J) is average breakage energy; δ^2 is variance of the log-normal distribution of the breakage energy.

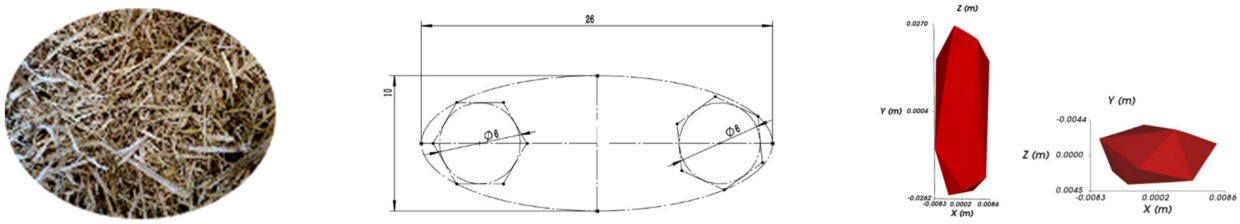
The relative breakage energy is calculated as follows:

$$e^* = \frac{e_{\max} e}{e_{\max} - e} \quad (6)$$

The average breakage energy is calculated as follows:

$$e_{50} = e_\infty \left[1 + \left(\frac{d_0}{L}\right)^\phi\right] \quad (7)$$

Rice straw was used as the experimental material, mainly composed of cellulose, hemicellulose and lignin, with a moisture content of 40–70%, a thickness of 5–10 mm and a length of 20–30 mm [32]. The stress-strain relationship of rice straw is following the generalized Hooke's law, and the breakage process is the same as that of the linear elastic material model. Assuming that the rice straw material parameters are linearly elastic, the Hertz-Milling bond contact model is adopted to analyze the rice straw particle fragmentation process, and energy consumption was calculated based on the forces and displacements of particle interactions during bond breakage [33]. The rice straw particle model usually is regarded as an axisymmetric ellipsoid in DEM simulations and is represented by a multi-sphere overlap connection method [34]. Based on the Tavares mathematical model, the rice particle model was simplified to an ellipsoid with a long axis of 52 mm and a short axis of 16 mm by measuring and calculating the dimensions of 100 rice straw particles. Further, regarding the irregular patterns of the straw particles, the straw particles were simulated as irregular polyhedra of 52 mm in length, 16 mm in width and 8 mm in height, as shown in Figure 7.



(**a**) (**b**) (**c**)

Figure 7. Modeling of rice straw particles. (**a**) Real straw particles; (**b**) straw particle simplification; (**c**) straw particle model.

Currently, only the JKR model (Johnson-Kendall-Roberts) can describe the surface interaction of elliptical contacts, where the shape of the JKR contact region changes throughout the contact [35]. In the JKR model, the line contact of different objects can be replaced by a cylindrical contact with an equivalent radius of curvature and a cylindrical contact with a bump. The contact between the straw particles can be replaced by line contact between two cylindrical surfaces with an equivalent radius of curvature. The equivalent model is shown in Figure 8. Based on the JKR model, the equivalent work was calculated according to the adhesion force between the straw particles, and the calculated value of the equivalent work was less than the ideal value, while the rough straw particle appearance caused the actual contact surface to be larger than the ideal contact surface [36].

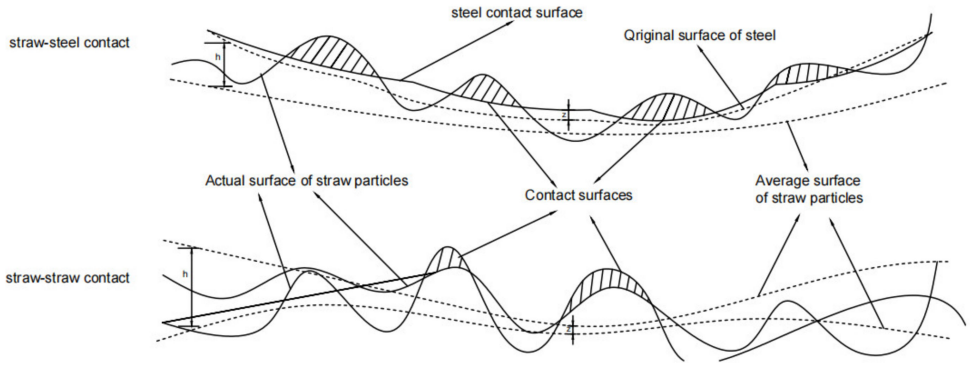


Figure 8. Surface contact equivalent model.

2.2.2. Parameter Setting

The parameters such as density, Poisson's ratio and shear elastic modulus of the straw particles and geometric model were set as shown in Table 1 [37].

Table 1. Setting of simulation parameters.

Straw particle	Density ρ/(kg/m^3)	1440
	Poisson ratio	0.25
	Shear elastic modulus G/(Pa)	1.5×10^6
Geometric model	Density ρ/(kg/m^3)	7800
	Poisson ratio	0.35
	Shear elastic modulus G/(Pa)	8×10^{10}
Particle-Particle	Recovery coefficient	0.65
	Static friction coefficient	0.18
	Rolling friction coefficient	0.01
Particle-Geometric mode	Recovery coefficient	0.65
	Static friction coefficient	0.15
	Rolling friction coefficient	0.01

2.2.3. Simulation Process

To find a suitable combination of spiral casing and tooth groove angle, different twin-screw structure combinations were designed for simulation analysis of pulping performance. The combination form of the spiral casing (P for positive spiral casing, N for negative spiral casing) and the arrangement form of tooth groove angle (W for 45°, S for 30°, R for 15°) are shown in Table 2.

Table 2. Combinations of spiral casing and arrangement of groove angle.

Spiral Sleeve Combination		Groove Angle Arrangement	
PNPN	NPPN	45°−30°−15° (WSR)	15°−45°−30° (RWS)
PPNN	PNNN	45°−15°−30° (WRS)	45°−45°−15° (WWR)
PNNP	NPNN	30°−45°−15° (SWR)	45°−45°−30° (WWS)
NPNP	NNPN	30°−15°−45°(SRW)	30°−30°−45° (SSW)
NNPP	NNNP	15°−30°−45° (RSW)	30°−30°−15° (SSR)

The number of straw particles was set to 2000, the rolling friction coefficient of particle-particle was 0.01, and the rolling friction coefficient of the particle-geometry model was 0.01. The computation step was set to 14 times, and the computation was terminated after 10 consecutive convergences, and the result was obtained after 8556 iterations to reach convergence. The simulation period of straw particles in the twin-screw pulping device was 21 s, intercepting the time points 0 s, 3 s, 6 s, 9 s, 12 s, 15 s, 18 s and 21 s of the combination breakage process for analysis. The straw particles have a certain viscosity that caused them to adhere to the twin-screw pulping device during the simulation process, which affected the accuracy of the simulation process. Therefore, the model was modified to ensure the accuracy of the model, as shown in Figure 9.

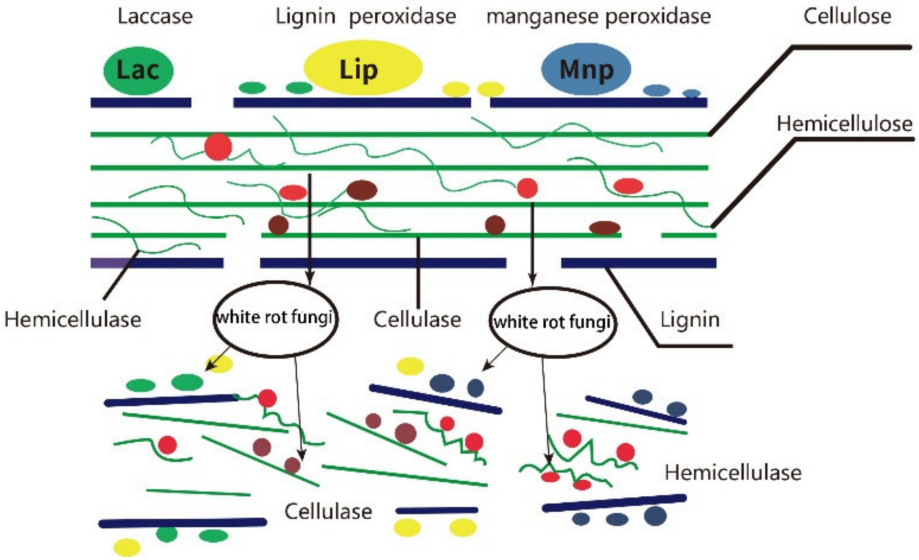


Figure 9. The mechanism of lignin degradation by white rot fungi.

2.3. Experimental Study

2.3.1. Trial Preparation

Rice straw was obtained from the experimental basement of the Shunbang Agricultural Machinery R&D Center in Siping City, Jilin Province, with a plant height of 0.7–1 m. Mature rice straw was selected and pre-treated to 5–10 cm straw by a kneading machine [38].

The CM0085 medium was sterilized at 121 °C for 30 min and cooled to room temperature. White rot fungi (Bio-114,230) were taken into the medium with an inoculation loop and were placed in a constant temperature vibration incubator and incubated continuously at 120 r/min for 7 days at 30 °C. The bacterial liquid was prepared by the expanded culti-

vation of white rot fungi and water in a ratio of 1:10 and sprayed evenly into the rice straw. The twin-screw pulping machine was operated and the microbiologically treated rice straw was pulped.

The mechanism of lignin degradation by white rot fungi is shown in Figure 9. A large number of extracellular oxidases were secreted during the mycelial growth and spread of white rot fungi, such as laccase (Lac), lignin peroxidase (Lip) and manganese peroxidase (MnP). The formation of H_2O_2 with the participation of molecular oxygen triggered the initiation of a series of free radical chain reactions to break the Cα-Cβ, β-O-4 and α-O-4 between the lignin benzene rings, followed by a series of reactions to degrade spontaneously.

Multi-factor test with tooth groove angle, screw speed and straw moisture content as influencing factors, and with pulp yield as an evaluation index of the performance of straw pulping [39]. Pulping yield is the percentage of pulp mass after lignin degradation of straw to the mass of straw before pulping, calculated as follows:

$$Q_e = \frac{G_2}{G_1} \times 100\% \quad (8)$$

where Q_e (%) is pulp yield; G_1 (g) and G_2 (g) are straw mass before pulping and pulp mass of straw after lignin degradation.

2.3.2. Box-Behnken Experimental Design

The ternary quadratic orthogonal center of rotation combination test was used to optimize the combination of tooth groove angle, screw speed and straw moisture content, and the factor codes are shown in Table 3.

Table 3. Factor coding.

Coding	Factors		
	Groove Angle A/(°)	Screw Speed B/(r/min)	Straw Moisture Content C/(%)
−1.682	15	450	55
−1	20	500	60
0	25	550	65
1	30	600	70
1.682	35	650	75

2.4. Validation Experiment

2.4.1. Twin-Screw Structure Verification Experiment

In order to find out the effect of twin-screw structure parameters on the straw pulping performance, the optimized design of the twin-screw pulping device was studied by the platform of Shunbang Agricultural Machinery Manufacturing Limited Company (Siping, China). The twin-screw pulping machine as shown in Figure 10.

The combination of the spiral casing of twin-screw pulping machine has a certain influence on the pulping performance [40]. Fibers passing through the twin screw machine always present a certain level of fibrillation and part of the hemicellulose and extractives would be removed [41]. The force of the positive spiral casing on the straw particles is the squeezing pressure, which is too strong for the bond between the straw particles and affects the degradation of the straw lignocellulose [42]. The force of the negative spiral casing on the straw particles is the shearing pressure, which is too strong for some of the straw particles attached to the side of the tooth groove, hindering the flow of straw materials. The arrangement of the tooth groove angle on negative spiral casing has a certain influence on the pulping performance [43]. If the angle of the tooth groove is too large, the shearing force on the straw is small and not enough to break the internal van der Waals force of the straw. If the angle of the tooth groove is too small, the straw material input is too small, and the straw material clearance is too large that the extrusion pressure on the straw is too small

to destroy the internal lignocellulosic component structure of the straw. Therefore, the experimental study of the twin-screw pulping performance was carried out by changing the combination of the spiral casing and the arrangement of the tooth groove angle on negative spiral casing.



Figure 10. Twin-screw pulping machine on location.

2.4.2. Straw Moisture Content Verification Experiment

The initial moisture content of rice straw was 40%, and the 36 groups of samples after different degrees of soaking treatment were put into high-temperature drying ovens and dried at a temperature of 105 °C for more than 12 h to obtain the dry mass of rice straw. The moisture content of the samples in real-time was calculated according to the rice straw moisture content formula [44], which is calculated as follows:

$$M_e = \frac{W_1 - W_2}{W_1} \times 100\% \quad (9)$$

where M_e (%) is moisture content of rice straw; W_1 (g) and W_2 (g) are mass of rice straw samples before drying and dry mass of rice straw samples.

The experimental study on the effect of straw moisture content on pulping performance was carried out by using the twin-screw pulping machine to pulping rice straw with moisture content of 50%, 55%, 60%, 65%, 70% and 75%, keeping the screw speed, tooth groove angle and pulping time consistent.

2.4.3. Screw Speed Verification Experiment

Set the twin-screw speed and use the cardboard press roll forming machine to make the pulping into straw board. Particularly, intercept 100 cm^2 of the straw board, using image recognition technology to calculate the number of stomata and trichome features of the straw board [45].

3. Results and Discussions

3.1. Simulation Results

From Figure 11a,b, it can be seen that at the beginning of the straw particles entering the twin-screw pulping device, the straw particles were in order and did not start to break. From Figure 11c,d, it can be seen that the straw particles entering the twin-screw conveying stage, the straw particles under the forward thrust and tangential force of the twin-screw, breaking the orderly arrangement of the state to irregular and disordered distribution, the friction between the straw particles made the initial breakage of the straw particles and began to accumulate breakage ratio energy. From Figure 11e,f, it can be seen that the straw particles started to enter the extrusion-shear stage with tighter distribution and were under

squeezing pressure from the positive spiral casing and shearing force from the negative spiral casing. The heat generated during the extrusion-shear stage could soften the lignin binding the fibers so that the hydrogen and covalent bonds between the bad cellulose and lignin could be easily broken [46]. The accumulated breakage ratio energy can resist part of the van der Waals force inside the straw particles and the straw particles started to break initially, yet the breaking effect is not obvious. From Figure 11g,h, it can be seen that the straw particles completely entered the pulping stage with a tight distribution and were under the pressure of the positive spiral casing and the shearing force of the negative spiral casing. The accumulated breakage ratio energy completely eliminated the van der Waals force inside the straw particles, and the straw particles broke rapidly in large quantities. Comparing and analyzing the number of broken straw particles, when the spiral casing combination form was NPNP and the angle arrangement of the negative spiral casing was WSR, the number of straw particles crushed was highest.

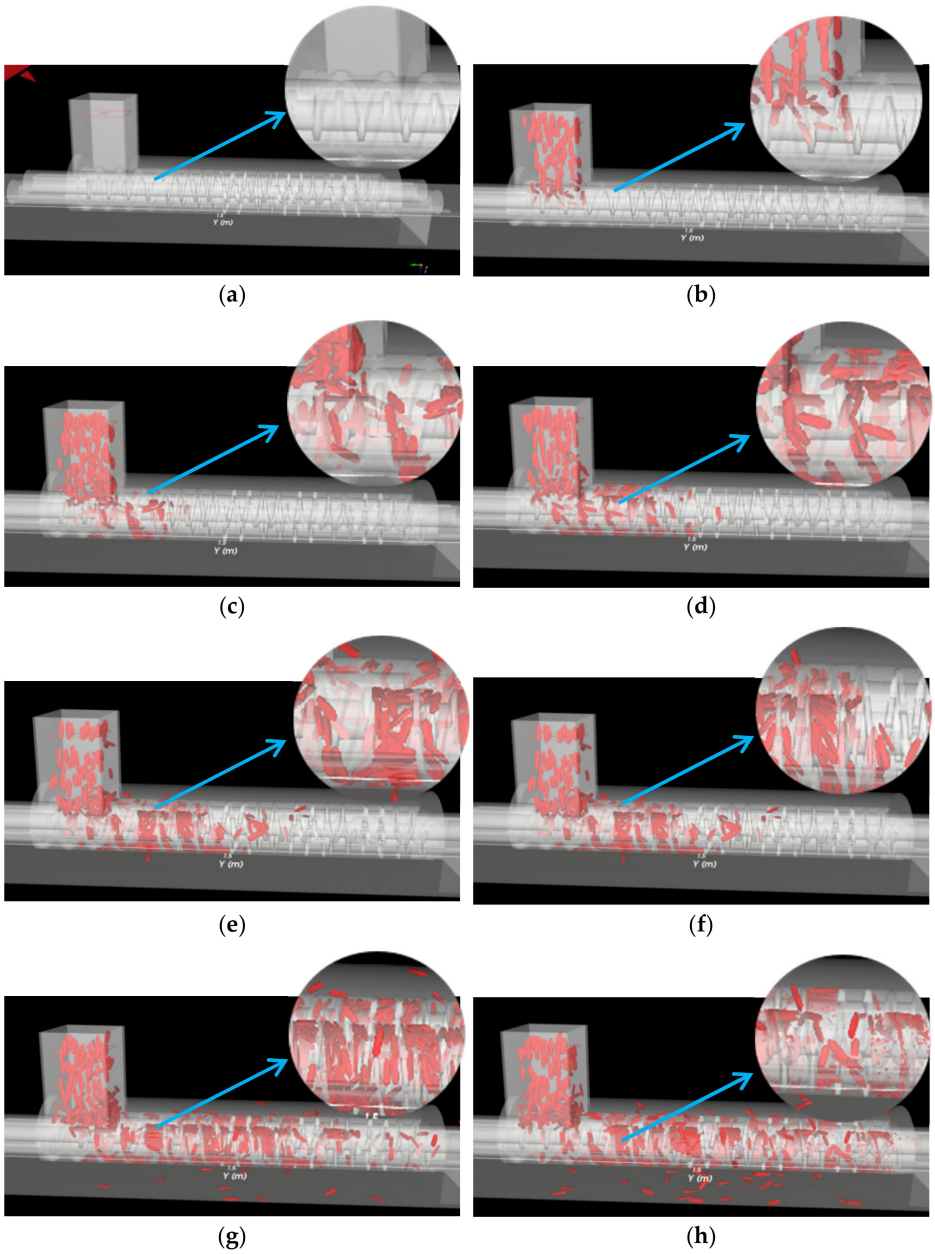


Figure 11. Simulation of breaking of straw particles in a twin screw machine for cellulose in time for 0 s (**a**), 3 s (**b**), 6 s (**c**), 9 s (**d**), 12 s (**e**), 15 s (**f**), 18 s (**g**) and 21 s (**h**).

3.2. Multi-Factor Experiment Results

3.2.1. Multi-Factor Experiment Results and Analysis

The experimental design was carried out with Design Expert 12.0 to analyze the factors to rationalize the data obtained from the experiment, as shown in Table 4.

Table 4. Analyzed factors of the experiment.

Number	Factors			
	Groove Angle A/(°)	Screw Speed B/(r/min)	Straw Moisture Content C/(%)	Pulping Yield/%
1	1	1	1	91.4
2	1	1	−1	82.8
3	1	−1	1	88.9
4	1	−1	−1	90.5
5	−1	1	1	89.3
6	−1	1	−1	86.7
7	−1	−1	1	88.3
8	−1	−1	−1	85.4
9	1.682	0	0	92.5
10	−1.682	0	0	84.2
11	0	1.682	0	89.3
12	0	−1.682	0	91.3
13	0	0	1.682	87.7
14	0	0	−1.682	92.1
15	0	0	0	83.4
16	0	0	0	85.5
17	0	0	0	87.4
18	0	0	0	90.9
19	0	0	0	89.6

A second-order regression model of the pulping performance with the three independent variables of tooth groove angle, screw speed, and straw moisture content was developed, its quadratic polynomial equation is:

$$\theta = 90.2 + 0.93\,A + 3.20\,B + 1.94\,C - 0.10\,AB - 0.03\,AC + 1.8\,BC - 7.86\,A^2 - 16.39\,B^2 - 7.21C^2 \quad (10)$$

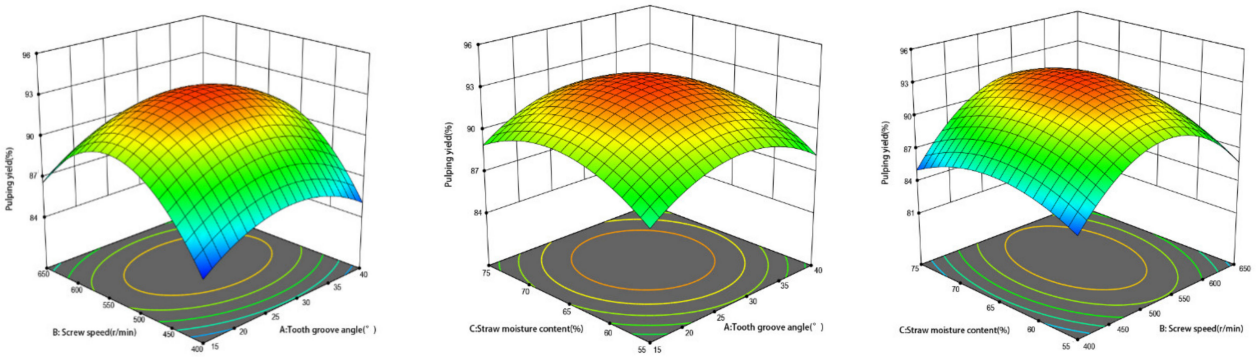
The results of the ANOVA are shown in Table 5 and the results showed that the equation model was highly significant with $p < 0.001$. The Lack of fit $p = 0.1239$ indicated that the equation fit was credible, reliable, and accurate. Tooth groove angle, screw speed, and straw moisture content had a highly significant effect on the pulping performance ($p < 0.01$). The interaction term BC had a significant effect on the pulping performance ($p = 0.0305$) and the secondary terms A^2, B^2 and C^2 had a significant effect on the pulping performance ($p < 0.05$). The order of influence of each factor on pulping performance is B > C > A.

3.2.2. Box-Behnken Experiment Results

The Box-Behnken experiment was designed to obtain the response surface graph of the interaction of tooth groove angle, screw speed, and straw moisture content on the pulping yield, as shown in Figure 12. The center of the response surface plane projection graph was located within the ellipse, indicating that the interactions AB, BC, and AC had a significant effect on the pulping performance.

Table 5. Analysis of variance of the Box-Behnken experiment.

Source	Sum of Squares	Freedom	Mean Square	*p*
Model	1894.46	9	210.5	<0.0001
A	7.03	1	7.03	0.0076
B	81.92	1	81.92	0.0035
C	30.03	1	30.03	0.0051
AB	0.04	1	0.04	0.9269
AC	0.0025	1	0.0025	0.9817
BC	12.96	1	12.96	0.0305
A^2	260.29	1	260.29	0.0001
B^2	1130.74	1	1130.74	<0.0001
C^2	219.03	1	219.03	0.0002
Residual	30.93	7	4.42	/
Lack of fit	22.57	3	7.52	0.1239
Error	8.36	4	2.09	/
Total value	1925.39	16	/	/



(**a**) (**b**) (**c**)

Figure 12. Response surface graph of the effect of interactions on straw the pulping rate. (**a**) The effects of screw speed (B) vs. tooth groove angle (A) on pulping yield; (**b**) the effects of straw moisture content (C) vs. tooth groove angle (A) on pulping yield; (**c**) the effects of straw moisture content (C) vs. screw speed (B) on pulping yield.

From Figure 12a, it was found that the pulp yield was 83.4% when the screw speed was 400 r/min and the tooth groove angle was 15°. Higher screw speed could increase the extrusion force and shear force on the straw and promote the production of extracellular oxidase by white rot fungi in straw and enhance the degree of lignin degradation. Lignin derivatives produced during lignin degradation could inhibit the hydrolysis of cellulase and xylanase, resulting in a relatively higher pulp yield [47]. The pulp yield was 85.5% when the screw speed was 650 r/min and the tooth groove angle was 15°. The larger tooth groove angle will lead to a larger opening area and smaller cross-sectional area, which will increase the feeding amount of the straw and improve the pulp yield.

From Figure 12b, it was found that the pulp yield was 84.2% when the straw moisture content was 55% and the tooth groove angle was 15°. With the increasing moisture content of straw, the internal van der Waals forces and chemical bonding of straw were gradually broken and the pulp yield improved. The pulp yield was 87.7% when the straw moisture content was 75% and the tooth groove angle was 15°. With the increasing angle of the tooth groove, the opening area increased and the cross-sectional area decreased, which improved the feeding amount and pulp yield.

From Figure 12c, it was found that the pulp yield was 82.8% when the screw speed was 400 r/min and the straw moisture content was 55%. With the increase of straw moisture content, free water was generated within the straw to fill the cell cavities, and the internal forces within the straw particles were easily broken leading to the improvement of pulp yield. The pulp yield was 85.4% when the screw speed was 400 r/min and the straw

moisture content was 75%. With the increase of screw speed, the twin-screw extrusion pressure and shear force on the straw gradually eliminated the internal van der Waals force of the straw. The lignin degradation rate was increased while the hydrolysis of cellulose and hemicellulose was inhibited and the pulp yield improved.

Straw pulping performance and pulp yield are positively correlated, that is, the straw pulping performance is the macro performance of the pulp yield. Higher pulping yield leads to better straw pulping performance [48].

3.3. Results of the Validation Experiment

3.3.1. Effect of Twin-Screw Structure Parameters on the Straw Pulping Performance

The experiment results are shown in Figure 13, the straw pulping performance was poor when the combination of the spiral casing was PNNN and NNNP, and the adjustment of the tooth groove angle failed to improve the straw pulping performance. The reason is that the number of positive spiral casings was large and the number of negative spiral casings was small, resulting in a larger squeezing force and smaller shearing force on the straw particles. Excessive squeezing pressure caused stronger bonding between straw particles and difficulty in breaking the hydrogen bond between cellulose and lignin, which hindered the degradation of straw lignocellulose and poor straw pulping performance. The straw pulping performance was poor when the spiral casing combination was NPNN and NNPN, while the straw pulping performance get improved when the tooth groove angle arrangement was SSR. The reason is that the small tooth groove angle and large cross-sectional area increased the shear force on the straw particles, making up for the small shear force of the spiral casing combination. It caused an easy disruption of the covalent bond between cellulose and lignin to improve the degradation of straw lignocellulose. However, the shear force was still not enough to break the internal van der Waals force of straw, and the straw pulping performance was also poor [49]. The straw pulping performance was poor when the spiral casing combination was PNNP and NPPN, while the straw pulping performance get improved when the tooth groove angle arrangement was SWR and RWS. The reason is that the angles of tooth groove were arranged as small-large-small, so that the straw material was first ground by large shear force, then flowed with higher flow, and finally ground by large shear force for the second time. The disadvantages of continuous shearing and continuous extrusion of the spiral casing combination were compensated, and the Cα-Cβ, β-O-4 and α-O-4 between the lignin benzene rings were broken to improve the straw pulping performance. The straw pulping performance was better when the combination of spiral casing was PPNN and NNPP, and the degradation of straw lignin was hindered with the combination of SSR and WWR in the tooth groove angle. The reason is that the angle of the tooth groove was continuously too large to small leading to a rapid decrement in flow, resulting in straw material blocking. The angle of the tooth groove was continuously small to large, resulting in the shearing force being too large to small, and the material feeding speed was too fast to grind the straw material completely, which affected the performance of straw pulping. The straw pulping performance was the best when the spiral casing combination was NPNP and PNPN, while the straw pulping performance get improved when the tooth groove angle arrangement was SSR. The reason is that the angle of the tooth groove was gradually smaller enabling the flow of straw material to decrease steadily, while the shearing force was increasing to grind straw more completely. It contributed to the cracking of the fiber surface and enhances the separation of the fiber material. The slowly changing material flow solved the problem of material blockage and achieved the optimal straw pulping performance.

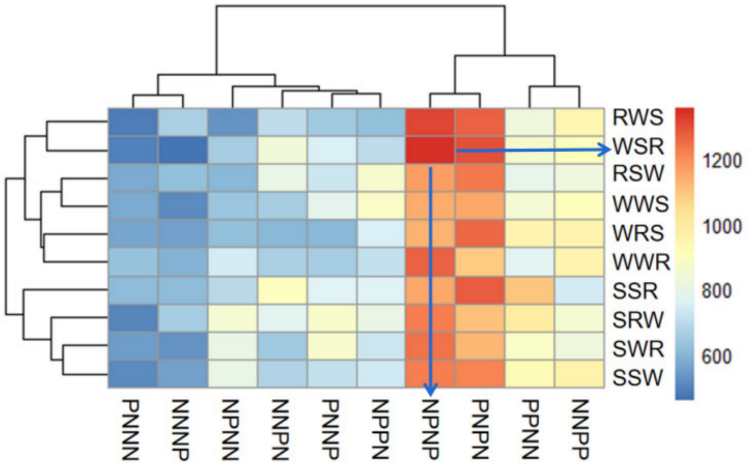


Figure 13. Influence of twin-screw structure parameters on the performance of straw pulping.

In summary, the straw pulping performance was the worst when the twin-screw pulping device spiral casing combination was PNNN and NNNP. The straw pulping performance was poor when the twin-screw pulping device spiral casing combination was NPNN and NNPN. The straw pulping performance was improved when the spiral casing combination was PNNP and NPPN and the tooth groove angle arrangement was SWR and RWS. The straw pulping performance was good when the spiral casing combination was PPNN and NNPP and the tooth groove angle arrangement was SSR and WWR. The straw pulping performance was the best when the spiral casing combination was NPNP and the tooth groove angle arrangement was WSR.

3.3.2. Effect of Straw Moisture Content on Pulping Performance

From Figure 14a, it was found that the straw slurry presented an inhomogeneous multi-angular agglomerate morphology, where the percentage of large multi-angular agglomerates was 65.4%. The reason is that when the straw moisture content was 50%, the internal force of the straw and the lignin benzene rings had not been destroyed and the straw fiber components were not separated so straw pulping performance was the worst [50]. From Figure 14b, it was found that the straw slurry presented inhomogeneous flat-ribbon agglomerate morphology, where the percentage of large inhomogeneous flat-ribbon agglomerates was 45.3%. The reason is that when the straw moisture content was 55%, part of the straw internal force was broken and the straw fiber component separation degree was low. The hydrogen bond between lignin and cellulose was only partially broken so the straw pulping performance was poor [51]. From Figure 14c, it was found that the straw slurry presented an inhomogeneous spherical agglomerate morphology, where the percentage of large spherical agglomerates was 25.7%. The reason is that when the straw moisture content was 60%, The activity of extracellular oxidase produced by white rot fungi that could degrade lignin was increased and the straw fiber components were separated to a higher degree so that the straw pulping performance was good. From Figure 14d, it was found that the straw slurry presented a homogeneous fine-grained agglomerate morphology, where the percentage of large fine-grained agglomerates was 6.5%. The reason is that when the straw moisture content was 65%, the straw internal forces were destroyed extremely high, and the more active oxidase triggered a series of free radical chain reactions that caused spontaneous degradation of the lignin benzene rings in a range of reactions. The straw fiber components were separated highly so that the straw pulping performance was the best. From Figure 14e, it was found that the straw slurry presented an inhomogeneous cottony agglomerate morphology, where the percentage of large cottony agglomerates was 16.8%. The reason is that when the water content of straw was 70%, the internal force of straw and the hydrogen bonds between lignin and cellulose were basically destroyed and the lignin in the straw fiber component was basically degraded

so that the straw pulping performance was good. From Figure 14e, it was found that the straw slurry presented an inhomogeneous thin-strip agglomerate morphology, where the percentage of large thin-strip agglomerates was 36.9%. The reason is that when the straw moisture content was 75%, the oxidase activity and the degradation of lignin benzene ring were decreased. Part of the straw internal forces had not been destroyed and the lignin degradation rate in the straw fiber component was reduced so that the straw pulping performance was poor.

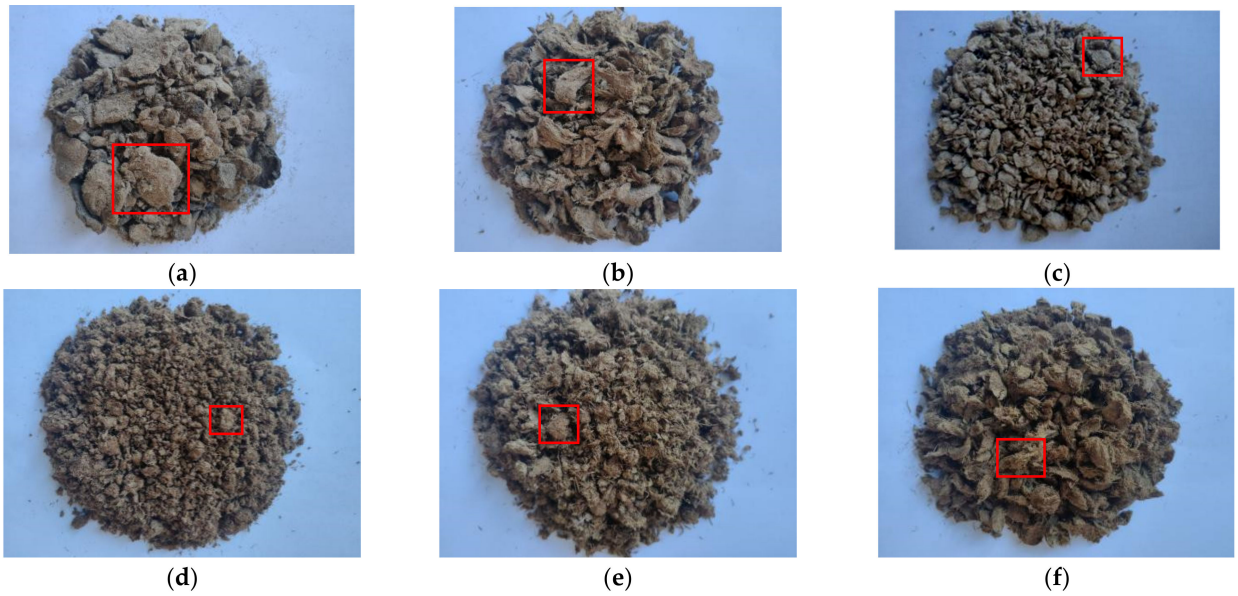


Figure 14. Illustration of straw pulp with different moisture content. Straw moisture content is 50% (**a**), 55% (**b**), 60% (**c**), 65% (**d**), 70% (**e**), and 75% (**f**).

In summary, when the straw moisture content was lower than 60%, only bound water existed inside the straw and the lack of free water to fill the cell cavity. The straw internal van der Waals force and chemical bonding were strong, and the lignin benzene rings were hardly broken leading to difficulty in breaking the straw. When the moisture content of straw was between 60 and 70%, the force within the straw was easily destroyed and the lignin benzene rings were easily disrupted by the effect of highly active lignin-degrading enzymes. The straw was broken to a strong degree resulting in good straw pulping performance. When the water content of straw was higher than 70%, the cell cavity of straw was filled with free water, the squeezing pressure and shear force on straw particles were buffered, and some of the van der Waals forces inside the straw were not destroyed. Part of the hydrogen bond between lignin and cellulose was not broken so some of the lignin was not degraded and the straw pulping performance turned poor. Therefore, the straw moisture content had a significant effect on the pulping performance, which was consistent with the simulation results.

3.3.3. The Effect of Screw Speed on Pulping Performance

From Figure 15a, it was found that part of the straw showed detachment from the main body with a high number of trichomes and rough straw fiber, including a total of 413 trichomes larger than 3 mm and 308 large blowholes. The reason is that when the screw speed was 450 r/min, the extrusion pressure and shear force on the straw failed to resist the van der Waals force inside the straw, and the lignin was not degraded resulting in poor pulping performance [52]. From Figure 15b, it was found that part of the straw fiber was attached to the surface of the slurry, the number of trichomes was relatively small and although the generally close but part of the straw fiber was rough, including 171 trichomes larger than 3 mm and 18 small blowholes. The reason is that when the screw speed was 500 r/min, the extrusion pressure and shear force on the straw eliminated most of the

internal van der Waals force of the straw. Cross-linking between fibers was broken and most of the lignin degradation led to better pulping performance. From Figure 15c, it was found that part of the straw fiber was slightly longer but the general straw fiber was close and evenly distributed, with a total of 84 trichomes larger than 3 mm and 10 blowholes. The reason is that when the screw speed was 550 r/min, the extrusion pressure and shear force on the straw basically eliminated the internal van der Waals force of the straw. The production of hair-like fibers on the fiber surface increased the surface area and the lignin basically degraded to allow the best pulp-making performance. From Figure 15d, it was found that part of the straw fiber stuck together into a block, and the straw fiber was rough and unevenly distributed, including 260 trichomes larger than 3 mm and 57 larger blowholes. The reason is that when the screw speed was 600 r/min, although the extrusion pressure and shear force on the straw eliminated part of the straw internal van der Waals force but the elimination effect was uneven. High-speed rotation inhibited the activity of lignin-degrading enzymes resulting in poor pulping performance.

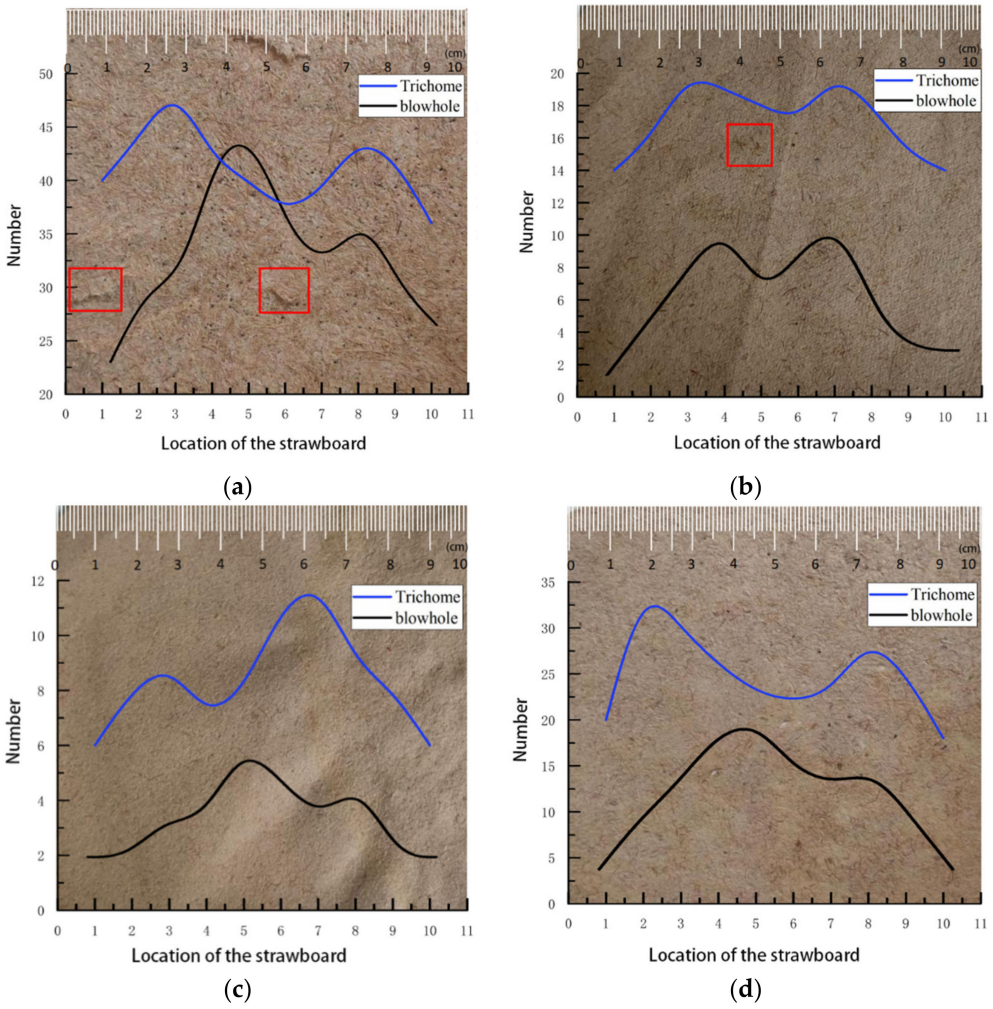


Figure 15. The pattern of trichomes and blowholes in the sheets achieved by different speeds of the screw. The speeds of the screw in (**a**–**d**) are 450 r/min, 500 r/min, 550 r/min and 600 r/min.

In summary, when the screw speed was lower than 500 r/min, the energy generated by the friction between the screw and the straw was lower than the straw breakage ratio energy, resulting in a large amount of unbroken straw and poor pulping performance. When the screw speed is higher than 550 r/min, the straw slurry blocked the twin-screw pulping device, which affected its lifetime. High-speed rotation inhibited the activity of lignin-degrading enzymes and led to a poor straw pulping performance. When the screw

speed was between 500 r/min and 550 r/min, the extrusion pressure and shear force on the straw were large and the broken straw fiber was small resulting in good straw pulping performance. Therefore, the screw speed had a significant effect on the pulping performance, which was consistent with the simulation results.

4. Conclusions

This work investigated the pulping performance of rice straw in a twin-screw machine for the rice straw treated with white rot fungi liquid by combining macroscopic and microscopic perspectives and ranking the role of different factors on the pulping performance. A simulation of straw particle breakage processes in twin-screw pulping machines based on the Tavares breakage model and straw particle fragments was produced by the Voronoi fracture equation; according to the distribution law of the Gaudin-Schumann function to calculate the fragmentation probability of straw particles, comparing and analyzing the number of broken straw particles with different combinations of twin-screw structure parameters. When the spiral casing combination is negative-positive-negative-positive (NPNP), the tooth groove angle arrangement of the negative spiral casing is $45°-30°-15°$ (WSR) and the moisture content of straw was 65%, the number of straw particle breakage is highest.

A ternary quadratic orthogonal center-of-rotation combination test was designed to establish a model between the pulp yield and the three independent factors of tooth groove angle, screw speed and straw moisture content. Multi-factor experiments showed that the order of the influencing factors on the pulp yield was screw speed > straw moisture content > tooth groove angle. When the screw speed is 550 r/min, the tooth groove angle is 30°, and the straw moisture content is 65%, the pulp yield reaches the highest value of 92.5%.

The straw pulping performance of the twin-screw pulping machine was verified, and the best pulping performance is achieved when the combination of the spiral casing of the twin-screw pulping machine is NPNP and the angle arrangement of the tooth groove is WSR. When the straw moisture content is 65%, the straw internal force is easily destroyed, and the straw pulping effect is good with a good straw broken degree. When the screw speed is 550 r/min, the extrusion pressure and shearing force of the twin screws on the straw is large, and the straw is finely broken leading to a good pulping performance. It shows that the experimental results are consistent with the simulation results and DEM can be used to study the analysis of the breakage process of straw and other materials.

Author Contributions: Conceptualization: D.R. and Y.G.; software, N.Z. and L.Z.; validation: H.C. and D.L.; supervisory role: D.R.; writing—review and editing: H.C.; funding acquisition and supervision: D.R. and Y.G. All authors have read and agreed to the published version of the manuscript.

Funding: This research was funded by the Educational Department of Liaoning Province (LSNQN202027).

Institutional Review Board Statement: Not applicable.

Informed Consent Statement: Not applicable.

Data Availability Statement: Not applicable.

Conflicts of Interest: The authors declare no conflict of interest.

References

1. Wang, W.; Lai, D.Y.; Sardans, J.; Wang, C.; Datta, A.; Pan, T.; Zeng, C.; Bartrons, M.; Peñuelas, J. Rice straw incorporation affects global warming potential differently in early vs. late cropping seasons in Southeastern China. *Field Crop. Res.* **2015**, *181*, 42–51. [CrossRef]
2. Liang, J.J. Analysis on Comprehensive Utilization of Straw in Agricultural Area. In Proceedings of the 7th ICASS International Conference on Social Science and Information (SSI 2018), Lima, Peru, 27–29 December 2018; pp. 30–34.
3. Hirani, A.H.; Javed, N.; Asif, M.; Basu, S.K.; Kumar, A. A review on first-and second-generation biofuel productions. In *Biofuels: Greenhouse Gas Mitigation and Global Warming*; Springer: New Delhi, India, 2018; pp. 141–154.
4. Sun, M.; Wang, Y.; Shi, L. Environmental performance of straw-based pulp making: A life cycle perspective. *Sci. Total Environ.* **2017**, *616–617*, 753–762. [CrossRef] [PubMed]

5. Weerasekara, N.S.; Powell, M.S.; Cleary, P.W.; Tavares, L.; Evertsson, M.; Morrison, R.; Quist, J.; de Carvalho, R. The contribution of DEM to the science of comminution. *Powder Technol.* **2013**, *248*, 3–24. [CrossRef]
6. Tavares, L.M.; André, F.P.; Potapov, A.; Maliska, C. Adapting a breakage model to discrete elements using polyhedral particles. *Powder Technol.* **2019**, *362*, 208–220. [CrossRef]
7. Tavares, L.M. Review and Further Validation of a Practical Single-Particle Breakage Model. *KONA Powder Part. J.* **2022**, *39*, 62–83. [CrossRef]
8. Barrios, G.K.; Jiménez-Herrera, N.; Tavares, L. Simulation of particle bed breakage by slow compression and impact using a DEM particle replacement model. *Adv. Powder Technol.* **2020**, *31*, 2749–2758. [CrossRef]
9. Tavares, L.M.; de Carvalho, R.M. Modeling breakage rates of coarse particles in ball mills. *Miner. Eng.* **2009**, *22*, 650–659. [CrossRef]
10. Oliveira, A.; Rodriguez, V.; de Carvalho, R.; Powell, M.; Tavares, L. Mechanistic modeling and simulation of a batch vertical stirred mill. *Miner. Eng.* **2020**, *156*, 106487. [CrossRef]
11. Tavares, L.M.; Rodriguez, V.A.; Sousani, M.; Padros, C.B.; Ooi, J.Y. An effective sphere-based model for breakage simulation in DEM. *Powder Technol.* **2021**, *392*, 473–488. [CrossRef]
12. Zeng, Y.; Mao, B.; Jia, F.; Han, Y.; Li, G. Modelling of grain breakage of in a vertical rice mill based on DEM simulation combining particle replacement model. *Biosyst. Eng.* **2022**, *215*, 32–48. [CrossRef]
13. Xu, T.; Zhang, R.; Wang, Y.; Jiang, X.; Feng, W.; Wang, J. Simulation and Analysis of the Working Process of Soil Covering and Compacting of Precision Seeding Units Based on the Coupling Model of DEM with MBD. *Processes* **2022**, *10*, 1103. [CrossRef]
14. Rahman, M.; Avelin, A.; Kyprianidis, K. An Approach for Feedforward Model Predictive Control of Continuous Pulp Digesters. *Processes* **2019**, *7*, 602. [CrossRef]
15. Garzon, L.; Fajardo, J.I.; Rodriguez-Maecker, R.; Fernandez, E.D.; Cruz, D. Thermo-Mechanical and Fungi Treatment as an Alternative Lignin Degradation Method for Bambusa oldhamii and Guadua angustifolia Fibers. *J. Fungi* **2022**, *8*, 399. [CrossRef] [PubMed]
16. Liu, T.Z.; Kittikunakorn, N.; Zhang, Y.; Zhang, F. Mechanisms of twin screw melt granulation. *J. Drug Deliv. Sci. Technol.* **2021**, *61*, 102150. [CrossRef]
17. Pradhan, S.U.; Sen, M.; Li, J.; Litster, J.D.; Wassgren, C.R. Granule breakage in twin screw granulation: Effect of material properties and screw element geometry. *Powder Technol.* **2017**, *315*, 290–299. [CrossRef]
18. Shirazian, S.; Darwish, S.; Kuhs, M.; Croker, D.M.; Walker, G. Regime-separated approach for population balance modelling of continuous wet granulation of pharmaceutical formulations. *Powder Technol.* **2018**, *325*, 420–428. [CrossRef]
19. Bumm, S.H.; White, J.L.; Isayev, A.I. Glass fiber breakup in corotating twin screw extruder: Simulation and experiment. *Polym. Compos.* **2012**, *33*, 2147–2158. [CrossRef]
20. Rol, F.; Belgacem, N.; Meyer, V.; Petit-Conil, M.; Bras, J. Production of fire-retardant phosphorylated cellulose fibrils by twin-screw extrusion with low energy consumption. *Cellulose* **2019**, *26*, 5635–5651. [CrossRef]
21. Theng, D.; Arbat, G.; Delgado-Aguilar, M.; Ngo, B.; Labonne, L.; Evon, P.; Mutjé, P. Comparison between two different pretreatment technologies of rice straw fibers prior to fiberboard manufacturing: Twin-screw extrusion and digestion plus defibration. *Ind. Crop. Prod.* **2017**, *107*, 184–197. [CrossRef]
22. Ho, T.T.T.; Abe, K.; Zimmermann, T.; Yano, H. Nanofibrillation of pulp fibers by twin-screw extrusion. *Cellulose* **2014**, *22*, 421–433. [CrossRef]
23. Kępa, K.; Chaléat, C.M.; Amiralian, N.; Batchelor, W.; Grøndahl, L.; Martin, D.J. Evaluation of properties and specific energy consumption of spinifex-derived lignocellulose fibers produced using different mechanical processes. *Cellulose* **2019**, *26*, 6555–6569. [CrossRef]
24. Espinosa, E.; Rol, F.; Bras, J.; Rodríguez, A. Production of lignocellulose nanofibers from wheat straw by different fibrillation methods. Comparison of its viability in cardboard recycling process. *J. Clean. Prod.* **2019**, *239*, 118083. [CrossRef]
25. Liang, F.; Fang, G.; Jiao, J.; Deng, Y.; Han, S.; Shen, K.; Shi, Y.; Li, H.; Zhu, B.; Pan, A.; et al. The Use of Twin Screw Extruder Instead of Model Screw Device During Bamboo Chemo-mechanical Pulping. *BioResources* **2018**, *13*, 2487–2498. [CrossRef]
26. Yang, X.; Wang, G.; Miao, M.; Yue, J.; Hao, J.; Wang, W. The Dispersion of Pulp-Fiber in High-Density Polyethylene via Different Fabrication Processes. *Polymers* **2018**, *10*, 122. [CrossRef]
27. Kratky, L.; Jirout, T. Modelling of particle size characteristics and specific energy demand for mechanical size reduction of wheat straw by knife mill. *Biosyst. Eng.* **2020**, *197*, 32–44. [CrossRef]
28. Yu, W.; Kai, W.; Yu, S. Effects of raw material particle size on the briquetting process of rice straw. *J. Energy Inst.* **2016**, *91*, 153–162.
29. Lenaerts, B.; Aertsen, T.; Tijskens, E.; De Ketelaere, B.; Ramon, H.; De Baerdemaeker, J.; Saeys, W. Simulation of grain–straw separation by Discrete Element Modeling with bendable straw particles. *Comput. Electron. Agric.* **2014**, *101*, 24–33. [CrossRef]
30. Molari, L.; Maraldi, M.; Molari, G. Non-linear rheological model of straw bales behavior under compressive loads. *Mech. Res. Commun.* **2017**, *81*, 32–37. [CrossRef]
31. Tavares, L.M. Analysis of particle fracture by repeated stressing as damage accumulation. *Powder Technol.* **2009**, *190*, 327–339. [CrossRef]
32. Liu, Y.; Li, Y.; Zhang, T.; Huang, M. Effect of concentric and non-concentric threshing gaps on damage of rice straw during threshing for combine harvester. *Biosyst. Eng.* **2022**, *219*, 1–10. [CrossRef]

33. Zhang, T.; Zhao, M.; Liu, F.; Tian, H.; Wulan, T.; Yue, Y.; Li, D. A discrete element method model of corn stalk and its mechanical characteristic parameters. *BioResources* **2020**, *15*, 9337–9350. [CrossRef]
34. Meng, X.; Han, Y.; Jia, F.; Chen, P.; Xiao, Y.; Bai, S.; Zhao, H. Numerical simulation approach to predict the abrasion rate of rice during milling. *Biosyst. Eng.* **2021**, *206*, 175–187. [CrossRef]
35. Zini, N.H.M.; de Rooij, M.B.; Bazr Afshan Fadafan, M.; Ismail, N.; Schipper, D.J. Extending the Double-Hertz Model to Allow Modeling of an Adhesive Elliptical Contact. *Tribol. Lett.* **2018**, *66*, 30. [CrossRef]
36. Zhang, T.; Peng, W.; Shen, K.; Yu, S. AFM measurements of adhesive forces between carbonaceous particles and the substrates. *Nucl. Eng. Des.* **2015**, *293*, 87–96. [CrossRef]
37. Zhang, S.; Ma, L.; Gao, S.; Zhu, C.; Yan, Y.; Liu, X.; Li, L.; Chen, H. A Value-Added Utilization Method of Sugar Production By-Products from Rice Straw: Extraction of Lignin and Evaluation of Its Antioxidant Activity. *Processes* **2022**, *10*, 1210. [CrossRef]
38. Jia, H.; Deng, J.; Deng, Y.; Chen, T.; Wang, G.; Sun, Z.; Guo, H. Contact parameter analysis and calibration in discrete element simulation of rice straw. *Int. J. Agric. Biol. Eng.* **2021**, *14*, 72–81. [CrossRef]
39. Lai, Y.-H.; Sun, H.-C.; Chang, M.-H.; Li, C.-C.; Shyu, J.-G.; Perng, Y.-S. Feasibility of substituting old corrugated carton pulp with thermal alkali and enzyme pretreated semichemical mechanical rice straw pulp. *Sci. Rep.* **2022**, *12*, 3493. [CrossRef]
40. Razzak, A.; Khiari, R.; Moussaoui, Y.; Belgacem, M.N. Cellulose Nanofibers from Schinus molle: Preparation and Characterization. *Molecules* **2022**, *27*, 6738. [CrossRef]
41. Rol, F.; Karakashov, B.; Nechyporchuk, O.; Terrien, M.; Meyer, V.; Dufresne, A.; Belgacem, M.N.; Bras, J. Pilot-Scale Twin Screw Extrusion and Chemical Pretreatment as an Energy-Efficient Method for the Production of Nanofibrillated Cellulose at High Solid Content. *ACS Sustain. Chem. Eng.* **2017**, *5*, 6524–6531. [CrossRef]
42. Guo, H.; Chang, J.; Yin, Q.; Wang, P.; Lu, M.; Wang, X.; Dang, X. Effect of the combined physical and chemical treatments with microbial fermentation on corn straw degradation. *Bioresour. Technol.* **2013**, *148*, 361–365. [CrossRef]
43. Taheri, H.; Hietala, M.; Oksman, K. One-step twin-screw extrusion process of cellulose fibers and hydroxyethyl cellulose to produce fibrillated cellulose biocomposite. *Cellulose* **2020**, *27*, 8105–8119. [CrossRef]
44. Robinson, J.; Aoun, H.K.; Davison, M. Determining moisture levels in straw bale construction. In Proceedings of the 3rd International Conference on Sustainable Civil Engineering Structures and Construction Materials—Sustainable Structures for Future Generations (SCESCM), Bali, Indonesia, 5–7 September 2016; pp. 1526–1534.
45. Lu, Z.; Hu, X.; Lu, Y. Particle Morphology Analysis of Biomass Material Based on Improved Image Processing Method. *Int. J. Anal. Chem.* **2017**, *2017*, 5840690. [CrossRef] [PubMed]
46. Hänninen, T.; Thygesen, A.; Mehmood, S.; Madsen, B.; Hughes, M. Mechanical processing of bast fibres: The occurrence of damage and its effect on fibre structure. *Ind. Crop. Prod.* **2012**, *39*, 7–11. [CrossRef]
47. Jing, X.; Zhang, X.; Bao, J. Inhibition Performance of Lignocellulose Degradation Products on Industrial Cellulase Enzymes During Cellulose Hydrolysis. *Appl. Biochem. Biotechnol.* **2009**, *159*, 696–707. [CrossRef]
48. Xing, L.; Xu, M.; Pu, J. The Properties and Application of an Ultrasonic-Assisted Wheat Straw Pulp having Enhanced Tendency for Ash Formation. *BioResources* **2016**, *12*, 871–881. [CrossRef]
49. Jiang, H.; Liu, J.; Wang, H.; Yang, R.; Zhao, W.; Yang, D.; Yin, S.; Shen, L. Study on Combined Vacuum–Mechanical Defoaming Technology for Flotation Froth and Its Mechanism. *Processes* **2022**, *10*, 1183. [CrossRef]
50. Nuengwang, W.; Srinophakun, T.R.; Realff, M.J. Real-Time Optimization of Pulp Mill Operations with Wood Moisture Content Variation. *Processes* **2020**, *8*, 651. [CrossRef]
51. Quispe-Quispe, L.G.; Limpe-Ramos, P.; Arenas-Chávez, C.A.; Gomez, M.M.; Mejia, C.R.; Alvarez-Risco, A.; Del-Aguila-Arcentales, S.; Yáñez, J.A.; Vera-Gonzales, C. Physical and Mechanical Characterization of a Functionalized Cotton Fabric with Nanocomposite Based on Silver Nanoparticles and Carboxymethyl Chitosan Using Green Chemistry. *Processes* **2022**, *10*, 1207. [CrossRef]
52. Gardea, F.; Glaz, B.; Riddick, J.; Lagoudas, D.C.; Naraghi, M. Energy Dissipation Due to Interfacial Slip in Nanocomposites Reinforced with Aligned Carbon Nanotubes. *ACS Appl. Mater. Interfaces* **2015**, *7*, 9725–9735. [CrossRef]